Accurate Gait Modelling based on Waveform Scaling before DFT

Yi Chiew Han [1*], Kiing Ing Wong [1], Iain Murray [2]

[1] Department of Electrical and Computer Engineering, Curtin University Malaysia, CDT250, Miri, Malaysia
[2] School of Engineering, Computing and Mathematical Sciences, Curtin University Australia, Perth, Australia
[*] yichiew@hotmail.com

Abstract: Gait modelling is essential for many applications including animation, activity recognition, medical diagnosis, and robotics. Many researchers have worked on mathematically express the movement of human bodies. At current stage, the reconstructed waveforms from the mathematical expressions either represent smoothened waveforms, noisy, or require high number of computations. In this paper, the thigh and shank angle waveforms are time and amplitude scaled before performing discrete Fourier transform (DFT). By doing so, the correlation coefficient between the original and reconstructed waveforms can be improved without increasing the number of harmonics. The shank's angular velocity is also recalculated from the reconstructed shank's angle waveform for gait phase detection, and shows accurate results in heel and toe strikes estimation when compared to the original shank's angular velocity. Additionally, the harmonic components of the waveforms are used for gait recognition. Experimental results show that it is useful to time and amplitude-scale the angle waveforms to "enlarge" the distinctive regions of the angle waveforms for better classification accuracy.

1. Introduction

Mathematical representation of different gait waveforms is useful in many gait applications including activity recognition and medical diagnosis. For example, Ibrahim et al. [1] compared the discrete cosine transform (DCT) coefficients of the hip's accelerometer signals to classify different walking patterns such as walking on flat surfaces, stairs, and ramps. Mostayed et al. [2] used the harmonic components of ankle-knee, knee-hip and hip-ankle angle waveforms to diagnose normal/abnormal gaits. Latt et al. [3] compared the acceleration patterns of the head and pelvis to detect gait abnormalities in patients with Parkinson's disease.

Gait modelling is also important for rehabilitation and robotics. In [4], a robotic assisted gait rehabilitation system is developed. In [5], normal gait pattern is generated for rehabilitation robots to avoid interaction forces between robot and human in case the patients walk correctly. In [6] and [7], walking pattern is generated for biped walking robots using human model.

Other applications of gait modelling include animation [8], biometric [9], and sports [10].

A lot of efforts had been done for gait modelling in recent years. Qiuyang et al. [11] and Wark et al. [12] represented the thigh angle waveforms and waist accelerometer signals based on Fourier series. Both [11] and [12] used linear predictive model to estimate the key harmonic components of the waveforms. Luu et al. [13] used neural networks to estimate the Fourier coefficient vectors of the lower limb joint angle waveforms. Sekine et al. [14] used discrete wavelet transform to approximate the signals of a tri-axial accelerometer attached to lower back. Hughes et al. [9] used genetic programming to perform symbolic regression for accelerometer data collected from smartphones placed in pockets.

However, it appears that the reconstructed waveforms based on the existing methods either represent smoothened waveforms [11] [12] [13] [14], or noisy [9] [15]. A problem with smoothened or fluctuating waveforms is that the altered waveforms can provide wrong or suffer loss of gait information. For example, gait sub-phases such as heel and toe strikes, can be identified using the local maxima or minima of the original waveforms [16] [17] [18].

Therefore, this research focuses on developing a method to model the angle waveforms accurately. This paper explores the use of proposed method to model the shank and thigh angle waveforms of people walking normally and abnormally. However, similar equations can be developed for waveforms originating from other body parts such as feet and hands.

We also attempt to recognize different types of gait patterns using the harmonic components of the shank and thigh angle waveforms to investigate if proposed method can improve the classification accuracy.

The remainder of this paper is structured as follows. Data collection method is stated in Section 2. The proposed method and its possible applications are de-scribed in Section 3. The results and discussion are in Section 4. Section 5 is the conclusion.

2. Data Collection

2.1. Inertial Measurement Unit (IMU)

Fig. 1. *Inertial Measurement Unit (IMU)*
(*a*) External view, **(b)** Internal view

Two Inertial Measurement Units (IMUs), as shown in Fig. 1, were constructed. Each IMU consists of a microcontroller Arduino Pro Mini 3.3V and a sensor

MPU6050. MPU6050 has a tri-axis accelerometer with ±2g range and a tri-axis gyroscope with ±250º/s range. Both sensors are time-synchronized and sampled at 100Hz with 16-bit resolution. All sensor data are transmitted to the thigh's IMU through wires, and then the thigh's IMU transmits all raw sensor data to a computer through wireless transceivers nRF24L01+. The IMUs are powered by 2 AAA batteries.

2.2. Experimental Setup

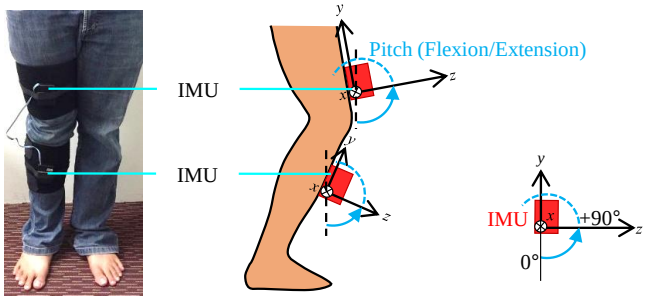

Fig. 2. *IMU placement*

Fig. 2 shows that the IMUs were strapped in front of the right thigh and shank using Velcro straps without any skin penetration. 20 healthy adults (male: 13; female: 7; age: 21-35; height: 151-182cm) were participated in the data collection. Each person was asked to walk normally at their own pace on a flat surface 3 times for 4-5 steps each trial (Walking pattern 1). A total of 263 nor-mal walking cycles was collected.

a *b*

Fig. 3. *Simulation of abnormal gaits*
(*a*) Bandaged knee. (***b***) Wearing an 8-cm height left shoe.

Additionally, we collected 3 types of simulated abnormal walking patterns to evaluate how well the pro-posed method generalizes to movement variability. 5 healthy adults (male: 3; female: 2; age: 22-32; height: 160-177cm; weight: 55-90kg) were involved. Firstly, each volunteer swung their right leg outwards while walking to simulate foot drop (Walking pattern 2). Then, the volunteers walked with bandaged knee, as shown in Fig 3(a), to simulate knee problem (Walking pattern 3). Finally, the volunteers wore an 8cm- height left shoe, as shown in Fig. 3(b), to simulate leg length discrepancy (Walking pattern 4). A total of 461 abnormal walking cycles were collected.

Ethical approval for this research is granted by Curtin University ethical review committee with approval number HRE2017-0834.

3. Data Processing

3.1. Gait Cycle Extraction

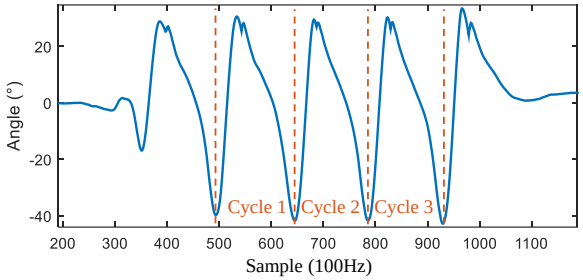

Fig. 4. *Gait cycle extraction using maximum backward swings of shank.*

Fig. 4 shows a shank angle waveform estimated using the method proposed in previous research [19] which had been validated against gold standard Vicon optical motion capture system. The same sensors, microcontrollers, and sampling period (100Hz) were used in [19] and in this research.

As shown in Fig. 4, we extract the gait cycles using the maximum backward swings of the shank. The gait cycles are extracted in such a way that it starts with a maximum backward swing of the shank, and ends with a subsequent maximum backward swing of the same shank.

3.2. Time and Amplitude Scaling before DFT

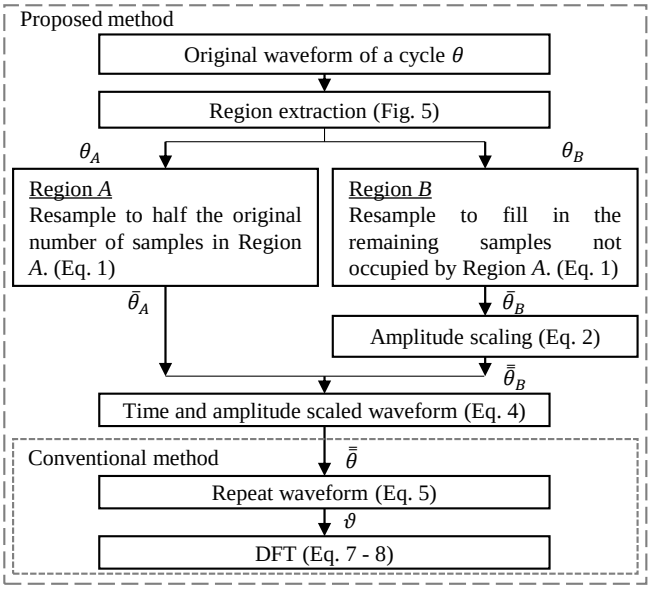

Fig. 5. *Flowchart for waveform scaling before DFT*

Fig. 5 shows the flowchart to time and amplitude scale the original waveforms before performing discrete Fourier transform (DFT), so that the required number of harmonics can be reduced while maintaining the accuracy.

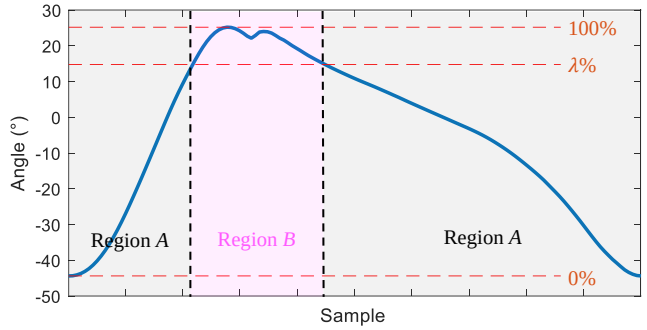

Fig. 6. *Region extraction for one cycle of an angle waveform*

As shown in Fig. 6, the angle waveform can be divided into 2 regions: smooth and less-smooth regions. The smooth region (Region *A*) is defined as the region where the angles are below a threshold λ% of the peak-to-peak angle. The less-smooth region (Region B) consists of more fluctuations and is defined as the region of the waveform above λ% of the peak-to-peak angle. Region *B* can also be called as the region-of-interest for some applications such as gait phase detection as it is where maximum swing, heel strike and toe strike occur [16] [17] [18].

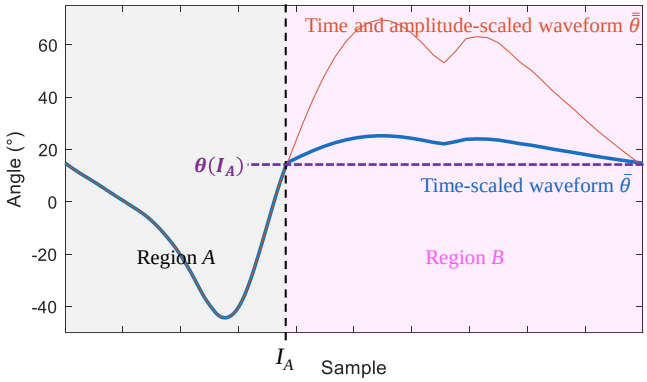

Remark: I_A and $\theta(I_A)$ are stored for waveform reconstruction.
- Region extraction of the time and amplitude-scaled waveform is achieved by finding the angle which is the closest to $\theta(I_A)$.
- The original length of Region *A* is $I_A/2$, while the original length of Region *B* is $1 - I_A/2$.

Fig. 7. *Time and amplitude-scaled waveforms*

After the regions are extracted, Region *A* is resampled to half of its original number of samples because Region *A* consists of a smoother curve compared to Region *B*, therefore downsampling Region *A* will not reduce much of the correlation coefficient (CORR). Then, Region *B* is resampled (time stretched) to fill in the remaining samples not occupied by Region *A*, as shown in Fig. 7. By doing so, the total number of samples of the resampled waveforms remain the same as the original waveform, and the non-smooth region can be zoomed in or focused before performing DFT.

As a side note, Region *A* could also be resampled to 1/3 or 1/4 of its original number of samples so that Region *B* could be further enlarged, but in this research we just resampled Region *A* to half to demonstrate the practicality of the proposed method. The resampling method in (1) can be used to resample the waveforms such that the original waveform with I number of samples is resampled to $\bar{I}$ number of samples.

$$\bar{\theta}_j = \theta_{i_{M1}+\left\lfloor \frac{j-1}{10}(i_{M2}-i_{M1}) \right\rfloor} \quad \text{for } j = 1,2,\cdots,11 \tag{1}$$

Where θ is the original waveform. $\bar{\theta}$ is the resampled waveform. ⌈ ⌉ and ⌊ ⌋ denote the ceiling and flooring functions, respectively.

However, the resampled/time-scaled waveform $\bar{\theta}$ (blue line in Fig. 7) has abrupt change of gradient at the connection point between Regions *A* and *B*. This can reduce the CORR between the original and reconstructed waveforms. To connect both regions smoothly, the amplitudes of resampled Region *B* $\bar{\theta}_B$ are multiplied with the ratio m of the final gradient of resampled Region *A* $\bar{\theta}_A$ to the initial gradient of $\bar{\theta}_B$, as stated in (2) and (3). $\bar{\theta}_A$ remain unchanged. The time and amplitude-scaled waveform $\bar{\bar{\theta}}$ (4) is shown with the red line in Fig. 7.

$$\bar{\bar{\theta}}_B(i) = \bar{\theta}_B(i) \times m - \bar{\theta}_B(1) + \theta(I_A) \tag{2}$$

$$m = \left| \frac{\bar{\theta}(I_A) - \bar{\theta}(I_A - 1)}{\bar{\theta}(I_A + 2) - \bar{\theta}(I_A + 1)} \right| \tag{3}$$

$$\bar{\bar{\theta}} = \left[\bar{\theta}_A \;\; \bar{\bar{\theta}}_B \right] \tag{4}$$

Where $\bar{\bar{\theta}}_B$ denotes the time and amplitude-scaled waveform of Region *B*, $\bar{\theta}_B(1)$ denotes the first sample of $\bar{\theta}_B$, I_A denotes the last sample of the resampled angle in Region *A*. $\theta(I_A)$ denotes the amplitude of the last angle of Region *A*.

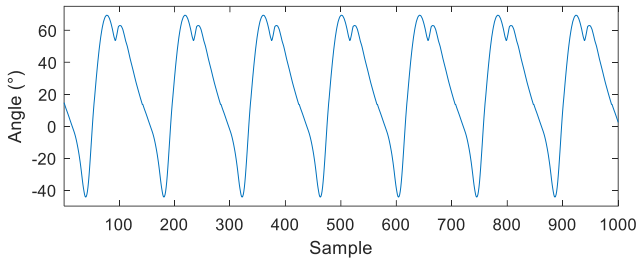

Fig. 8. *Time and amplitude-scaled waveform repeated n times*

The time and amplitude-scaled waveform $\bar{\bar{\theta}}$ is then then repeated *n* times as shown in Fig. 8. In this research, *n* is selected to be 15 for the repeated waveform ϑ (5). The harmonics are more distinctive to be identified as n increases.

$$\vartheta = [\bar{\bar{\theta}} \;\; \bar{\bar{\theta}} \;\; \bar{\bar{\theta}} \;\; \cdots \;\; \bar{\bar{\theta}}] \tag{5}$$

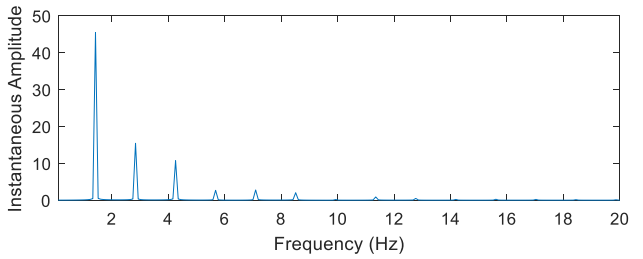

Fig. 9. *Single-sided amplitude spectrums of a full cycle of scaled waveform.*

DFT in (6) is performed for the repeated waveform ϑ and resulted in Fig. 9. The DFT of the scaled waveform at h^{th} harmonic can be expressed as (7).

$$DFT_n = \frac{2}{L}\sum_{i=1}^{L} \vartheta_i e^{-j2\pi(i-1)\frac{n-1}{L}} \quad \text{for } n = 1,2,\cdots,\frac{L}{2} \tag{6}$$

$$DFT_h = \frac{2}{L}\sum_{i=1}^{L} \vartheta_i e^{-j2\pi(i-1)\frac{h}{T}} \quad \text{for } h = 1,2,\cdots,H \qquad (7)$$

Where the transform length is selected to be the same as the length $L \approx 1500$ of ϑ. e denotes the exponential function, and j is the imaginary number. H denotes the total number of harmonics. I is the number of samples of $\bar{\bar{\theta}}$.

The instantaneous amplitude α_h and the phase φ_h of the h^{th} harmonic can be obtained by writing the DFT in polar form (8).

$$DFT_h = \alpha_h \angle \varphi_h \qquad (8)$$

The DC component b of the time and amplitude-scaled waveform can be obtained by calculating the average value of the waveform within one period.

3.3. Waveform Reconstruction

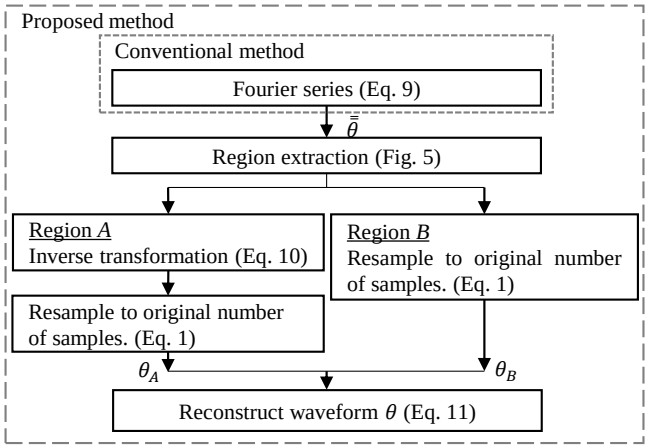

Fig. 10. *Flowchart to reconstruct the waveform*

Fig. 10 shows the flowchart to reconstruct the angle waveform θ. The scaled waveform $\bar{\bar{\theta}}$ can be reconstructed by inputting the instantaneous amplitudes α_h and phase φ_h of the h^{th} harmonics to Fourier series in (9).

$$\bar{\bar{\theta}}(i) = b + \sum_{h=1}^{H} \alpha_h \cos(2\pi h i + \varphi_h) \qquad (9)$$

Where b denotes the average value of the scaled waveform within one period.

Regions A and B are then extracted by finding the closest scaled angle $\bar{\bar{\theta}}$ to $\theta(I_A)$. See the remark in Fig. 7.

The scaled angles of Region B $\bar{\bar{\theta}}_B$ can be inverse-transformed back to its original amplitudes according to (10).

$$\bar{\theta}_B(i) = \frac{\bar{\bar{\theta}}_B(i) - \bar{\bar{\theta}}_B(1)}{m} + \theta(I_A) \qquad (10)$$

Where m is stored from (3) for waveform reconstruction.

After that, both regions are resampled back to its original length. The original length of Region A is I_A, while the original length of Region B is $100 - I_A$.

The reconstructed waveform θ can be obtained by appending θ_B to θ_A, as stated in (11).

$$\theta = [\theta_A \ \ \theta_B] \qquad (11)$$

3.4 Possible Application 1: Gait Phase Detection

Existing literature show that the distance between the sacrum and heel [20], the distance between ankle and heel [21], and horizontal velocity [20]-[22] can be used to detect the heel strike and toe off. These existing methods, although accurate, rely on expensive and non-portable optical motion capture system for data collection.

Another accurate method for gait phase detection is using force sensors to measure the forces exerted by the heel and toe during walking [23]. Force plates are usually available only in the laboratory. Force sensitive resistors, although portable, would require the users to place the sensors under the foot at correct positions, and this may bring discomfort to the users while walking.

Recently, inertial sensors are used to detect the gait phases [24] [25]. Inertial sensors are not only low cost and portable, but widely available in smartphones. Based on [24] and as shown in Fig. 11, the normal heel strike can be estimated using the first local maximum of shank's angular velocity ω. The normal toe strike can be estimated using the first local maximum filtered angular velocity $\bar{\omega}$. The toe off can be estimated using the last local maximum of ω.

In this experiment, we attempt to reconstruct the shank's angular velocity ω from the reconstructed waveform of the shank angle θ to show that proposed gait modelling method could retain the gait phase information better than conventional method. The angular velocity and its moving average can be obtained from (12) and (13), respectively.

$$\omega_i = \frac{\theta_i - \theta_{i-1}}{T} \qquad (12)$$

$$\bar{\omega}_i = \frac{1}{2k}\sum_{i=i-k}^{i+k} \omega_i \qquad (13)$$

where T is the sampling period. Constant k is set as 10 similar to [24] which uses the same sensors.

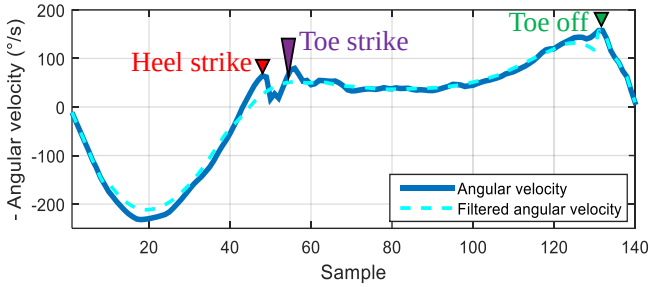

Fig. 11. *Shank's angular velocity to detect gait phases.*

3.5 Possible Application 2: Gait Recognition

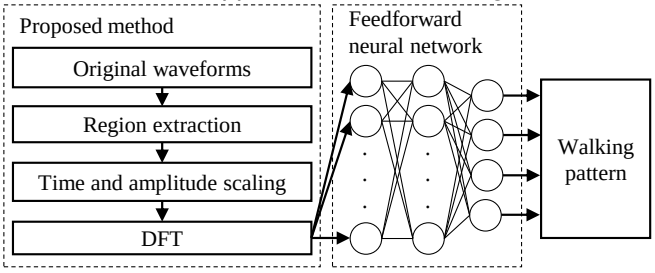

Fig. 12. *Applying proposed method for gait recognition.*

In [2], harmonic components of the ankle-knee, knee-hip and hip-ankle angle waveforms were used classify

normal/abnormal gaits. To see if the proposed method can be used to improve the classification accuracy compared to conventional method, a simple fully connected neural network, as shown in Fig. 12, is utilized. 4 different types of gait patterns (1 normal, 3 abnormal) were collected and to be classified. The input features are the instantaneous amplitudes α_h, phase φ_h and average value b of the shank and thigh angle waveforms when H=10. The initial weights and biases are random, and updated with backpropagation. The neural network is set to have 1 to 3 hidden layers with different numbers of neurons. The activation function used is a hyperbolic tangent function. For balanced training dataset, 50 gait cycles from each pattern are used for training while the remaining gait cycles are used for testing. The training to validation ratio is 80:20%. For the proposed method, a pre-set threshold $\lambda = 0.55$ is used to extract distinct regions of the 4 different types of walking patterns.

4. Results & Discussions

The proposed method pre-scales the original waveforms before applying DFT. Conventional method in this paper means applying DFT without pre-scale the waveforms, as labelled in Fig. 5 and 10.

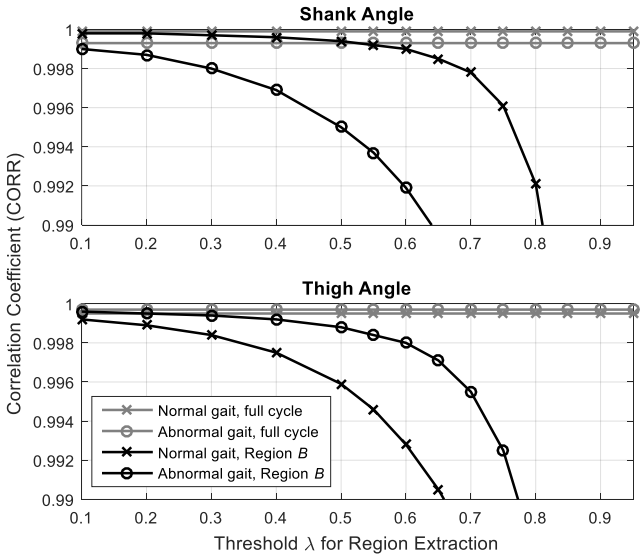

Fig. 13. *Plot of mean CORR against thresholds λ for conventional method when H=6.*

In [11] and [13], 6 harmonic components were used to predict the angle waveforms. In [15], 5 harmonic components were used. When checked with the experimental results, the overall (full cycle) CORR based on conventional method is indeed high above 0.999 when the number of harmonics H=6. However, as shown in Fig. 13, when checked specific regions (Region B) of the reconstructed waveforms by varying the thresholds λ, the CORR of the conventional method at Region B is low (<< 0.999) when H=6. This indicates that 6 harmonics are insufficient to represent the angle waveforms accurately based on conventional method.

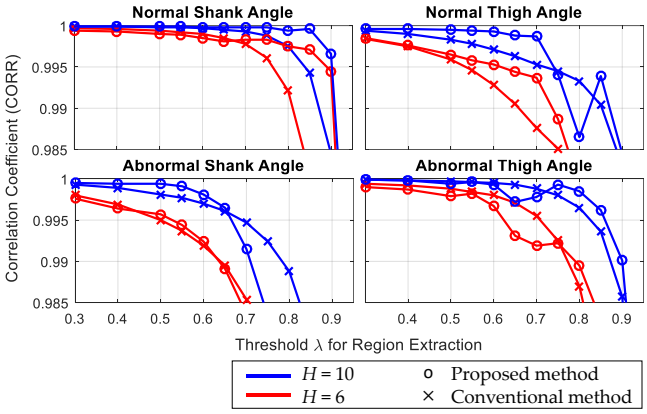

Fig. 14. *Plot of mean CORR at Region B against thresholds λ when H=6 and 10.*

A good choice of threshold λ is crucial in maintaining a highly accurate mathematical representation of an angle waveform based on proposed method. The ideal value of λ should successfully extract the waveform in such a way that Region B consists of mainly the less-smooth region. As shown in Fig. 14, a low value of λ (<0.5) will not help much in increasing the CORR because the extracted Region B consists of a big portion of smooth waveform. We cannot set λ to be too high as this will reduce the CORR because most of the less-smooth region is failed to be captured.

Referring to Fig. 14, λ for the proposed method are set as 0.85, 0.70, 0.55, and 0.75 for normal shank, normal thigh, abnormal shank, and abnormal thigh angle waveforms, respectively. This is because these λ values result in a high CORR and great improvement in CORR compared to conventional method, which means Region B averagely consists most of the less-smooth region of the waveforms at these thresholds.

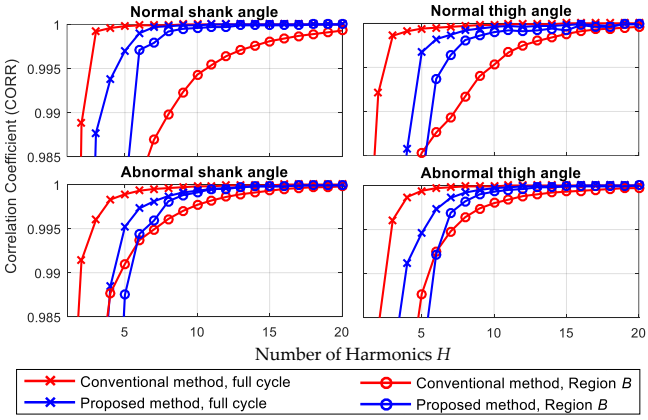

Fig. 15. *Plot of mean CORR against H.*

Table 1 Mean CORR between Original and Reconstructed Angle Waveforms

Angle	Number of Harmonics *H*	Conventional Method		Proposed Method	
		Full Cycle	Region *B*	Full Cycle	Region *B*
Normal shank	3	0.9992	**0.9284**	0.9877	**0.8772**
	6	0.9999	**0.9822**	0.9990	**0.9971**
	10	1.0000	**0.9943**	0.9999	0.9996
	15	1.0000	**0.9981**	1.0000	0.9999
	20	1.0000	0.9993	1.0000	1.0000
	25	1.0000	0.9997	1.0000	1.0000
Normal thigh	3	**0.9986**	**0.9767**	**0.9708**	**0.7480**
	6	0.9995	**0.9876**	0.9982	**0.9937**
	10	0.9998	**0.9953**	0.9996	0.9990
	15	1.0000	**0.9988**	0.9998	0.9992
	20	1.0000	0.9996	0.9999	0.9999
	25	1.0000	0.9998	1.0000	1.0000
Abnormal shank	3	**0.9960**	**0.9752**	**0.9664**	**0.8737**
	6	0.9993	**0.9937**	0.9973	**0.9944**
	10	0.9998	**0.9977**	0.9993	0.9991
	15	0.9999	0.9993	0.9995	0.9980
	20	1.0000	0.9998	0.9999	0.9999
	25	1.0000	0.9999	1.0000	1.0000
Abnormal thigh	3	**0.9961**	**0.9557**	**0.9799**	**0.9422**
	6	0.9997	**0.9925**	0.9973	**0.8876**
	10	0.9999	**0.9980**	0.9997	0.9993
	15	1.0000	0.9993	0.9999	0.9999
	20	1.0000	0.9997	0.9983	1.0000
	25	1.0000	0.9999	1.0000	1.0000

Values in bold font means less than 0.9990 CORR.

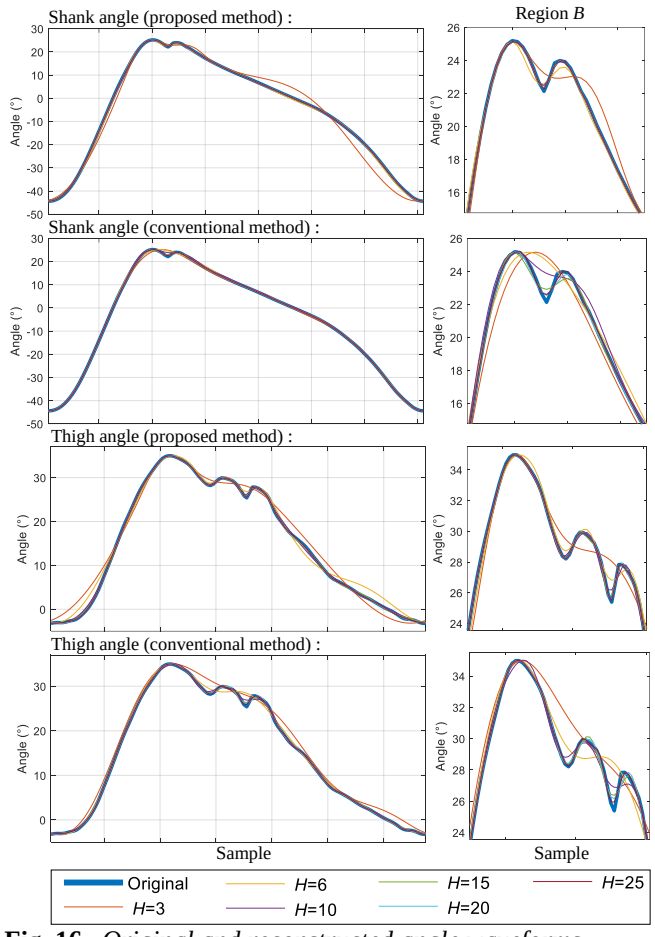

Fig. 16. *Original and reconstructed angle waveforms.*

Fig. 15 shows a plot of mean CORR against *H*. Considering the full cycle, the mean CORR of the proposed method (blue cross line) is lower than the conventional method (red cross line) when $H<10$. However, when $H\geq10$, the mean CORR of the full cycle for both conventional and proposed methods are about the same (≥0.999). Considering only the Region *B*, the proposed method (blue circled line) has higher mean CORR than conventional method (red circled line) when $H>6$.

As listed in Table 1, the conventional method when $H\leq6$ has low mean CORR at Region *B* <0.990 and <0.994 for normal and abnormal angle waveforms, respectively. The mean CORR at Region *B* improved to around 0.995 and 0.998 when $H=10$. As a comparison, the proposed method when $H=10$ has achieved a high mean CORR around 0.999 at Region *B*. It is only when $H>15$, the conventional method achieves a high mean CORR above 0.999 at Region *B*, but the idea is to represent the waveforms accurately using lesser *H*.

As shown in Fig. 16, the reconstructed waveforms based on conventional method when $H \leq 10$ and proposed method when $H \leq 6$ represent smoothened original waveforms. The reconstructed waveforms based on proposed method when $H=10$ represent the original waveforms more accurately than conventional method when $H=15$ at Region *B*.

Comparing with existing methods, it can be seen from the figures provided in the existing literatures that the reconstructed waveforms based on the existing methods either represent smoothened waveforms [11] [12] [13] [14], or noisy [9] [15].

$$DFT_h = \sum_{i=1}^{L} k_1 \vartheta_i e^{j(k_2 h)(i-1)}$$

L cosine function
L sine function
$e^{jx} = \cos(x)+j\sin(x)$
$2L$ multiplications
L complex multiplications
L complex additions
$k_1 = \frac{2}{L}$
$k_2 = -0.02\pi$
$L \approx 1500$ is the length of the repeated waveform ϑ.

Fig. 17. *Number of computations required per harmonic.*

Table 2 Approximate number of computations required

Number of Harmonics *H*	Additions	Multiplications	Cosine/Sine Function
1	2*L*	4*L*	2*L*
4	8*L*	16*L*	8*L*
5	10*L*	20*L*	10*L*
7	14*L*	28*L*	14*L*
10	20*L*	40*L*	40*L*
14	28*L*	56*L*	28*L*

$L \approx 1500$ is the length of repeated waveform. 1 complex addition = 2 additions. 1 complex multiplication = 2 multiplications.

The proposed method when $H=10$ averagely achieves the same CORR as conventional method when H =

24, 17, 14, and 15 for normal shank, normal thigh, abnormal shank, and abnormal thigh angle waveforms, respectively. This means a reduction of 14, 7, 4, and 5 DFT calculations in (7) to achieve the same CORR.

Fig. 17 counts the number of computations required to run (7) per harmonic. As stated in Table 2, the total number of computations saved for 14, 7, 4, and 5 harmonics is 112L, 56L, 32L, and 40L, respectively. The proposed waveform scaling method in (2)-(3) uses around 202 additions and 101 multiplications. Adding with the computations required to extract the regions (Fig. 6) and scaling the waveform (Fig. 7), the computations required are far lesser than an $L \approx 1500$.

Table 3 Possible Application 1: Gait Phase Detection (Mean Absolute Error in Sample Difference)

H	Heel strike		Toe strike		Toe off	
	Conv.	Prop.	Conv.	Prop.	Conv.	Prop.
6	5.82	1.33	2.99	0.87	3.19	7.73
10	4.29	0.73	2.06	0.47	2.67	3.74
15	2.33	0.35	1.21	0.32	2.03	3.00
20	1.33	0.36	0.48	0.22	1.70	2.75
25	1.13	0.29	0.36	0.16	1.52	2.36

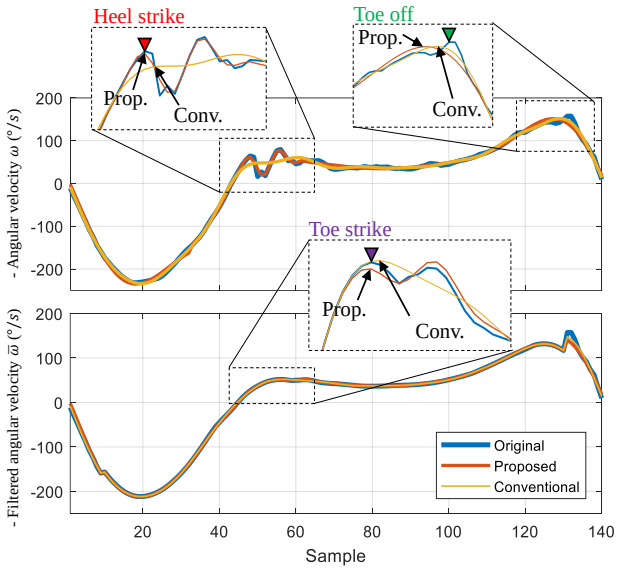

Fig. 18. *Shank's angular velocity to detect gait phases.*

Fig. 18 shows the shank's angular velocity estimated by differentiating the shank's angle when H=10 (12). The heel and toe strikes can be detected very accurately using the shank's angular velocity reconstructed from the angles based on proposed method. The shank's angular velocity reconstructed from the conventional method gives higher error in heel and toe strikes detections. This indicates that the proposed method has successfully retained the heel and toe strikes information. As listed in Table 3, the proposed method when H=10 has lower mean absolute error than conventional method when H=25 and 20 for heel and toe strikes detections, respectively.

However, the proposed method gives higher mean absolute error of about +1 sample difference (+10ms) than conventional method in estimating the toe off. This is because the toe off is in Region *A*, while the proposed method is focusing on improving the CORR in Region *B* which consists of heel and toe strikes. To solve this, future work can consider extracting more than two regions and focusing on improving the CORR in multiple regions rather than just one Region *B*.

Table 4 Possible Application 2: Gait Recognition (Testing Accuracy in %)

N	Pattern	True Positive		True Negative		Accuracy	
		Conv.	Prop.	Conv.	Prop.	Conv.	Prop.
15	1	100	100	97.04	98.60	97.78	98.95
	2	92.16	82.35	91.50	88.89	91.67	87.25
	3	62.50	92.86	86.90	95.83	80.80	95.09
	4	80.95	80.95	93.12	92.59	90.08	89.68
	Mean	**83.90**	**89.04**	**92.14**	**93.98**	**90.08**	**92.74**
15, 8	1	99.07	100	99.22	98.60	99.18	98.95
	2	80.39	88.24	90.20	92.81	87.75	91.67
	3	82.14	91.07	92.86	97.02	90.18	95.54
	4	76.19	79.37	92.59	89.95	88.49	87.30
	Mean	**84.45**	**89.67**	**93.72**	**94.59**	**91.40**	**93.36**
20, 15, 8	1	100	100	99.84	100	99.88	100
	2	78.43	80.39	91.50	90.85	88.24	88.24
	3	78.57	94.64	92.86	95.24	89.29	95.09
	4	76.19	87.30	92.59	93.65	88.49	92.06
	Mean	**83.30**	**90.58**	**94.20**	**94.93**	**91.47**	**93.85**

N = [20,15,8] means there are three hidden layers in the neural network with 20, 15 and 8 neurons in the first, second and third layer, respectively. The reported testing accuracies are the best accuracies out of 100 trials.

It is demonstrated in Table 4 that waveform scaling before DFT can increase the true positive rate of the gait multi-class classification by 5-7% when compared to the conventional method. The original waveforms with no waveform scaling give lower accuracy than the proposed method with waveform scaling in classification task. In term of medical application, the proposed approach is expected to work on cohorts with gait impairments (e.g. stroke and Parkinsonian gait) as experimental results show that it is useful to time and amplitude-scale the angle waveforms to "enlarge" the distinctive regions of the angle waveforms for better classification accuracy. Autonomous gait diagnosis system with better accuracy could be developed to assist the clinicians in early diagnosis.

5. Conclusion

A method to mathematically represent the shank and thigh angle waveforms accurately without smoothening and fluctuations is proposed. The proposed method has also been tested with simulated abnormal gait patterns. The CORR between the original and reconstructed waveforms is increased without increasing the number of harmonics. By reducing the number of harmonics without reducing the accuracy, the calculations for DFT can be reduced. It is shown that the proposed method when H=10 averagely achieves the same CORR as conventional method when H = 24, 17, 14, and 15 for normal shank, normal thigh, abnormal shank, and abnormal thigh angle waveforms, respectively. This means a reduction of 4 to 14 DFT computations to achieve the same CORR. As the reconstructed waveforms based on proposed method represent the original waveforms accurately, the reconstructed waveforms are suitable for gait analysis such as gait phase detection. It is also demonstrated that the harmonic components of the waveforms based on proposed method can be used to increase the gait classification accuracy when distinctive regions of the waveforms are extracted. Future

works include but not limited to extracting multiple regions, improving how the regions are being extracted, and resampling the regions with different ratios.

6. References

[1] R. K. Ibrahim, E. Ambikairajah, B. Celler, N. H. Lovell and L. Kilmartin, "Gait patterns classification using spectral features," *IET Irish Signals and Systems Conference (ISSC 2008)*, Galway, 2008, pp. 98-102. doi: 10.1049/cp:20080645

[2] A. Mostayed, M. Mynuddin, G. Mazumder, Sikyung Kim and Se Jin Park, "Abnormal Gait Detection Using Discrete Fourier Transform," *2008 International Conference on Multimedia and Ubiquitous Engineering (mue 2008)*, Busan, 2008, pp. 36-40. doi: 10.1109/MUE.2008.59

[3] M. D. Latt *et al*, "Acceleration Patterns of the Head and Pelvis During Gait in Older People With Parkinson's Disease: A Comparison of Fallers and Nonfallers," *The Journals of Gerontology,* vol. 64A, *(6),* pp. 700-6, 2009. doi: 10.1093/gerona/glp009

[4] H. B. Lim, K. H. Hoon, Y. C. Soh, A. Tow and K. H. Low, "Gait planning for effective rehabilitation - From gait study to application in clinical rehabilitation," *2009 IEEE International Conference on Rehabilitation Robotics*, Kyoto, 2009, pp. 271-276. doi: 10.1109/ICORR.2009.5209599

[5] H. Vallery, E. H. F. van Asseldonk, M. Buss and H. van der Kooij, "Reference Trajectory Generation for Rehabilitation Robots: Complementary Limb Motion Estimation," in *IEEE Transactions on Neural Systems and Rehabilitation Engineering*, vol. 17, no. 1, pp. 23-30, Feb. 2009. doi: 10.1109/TNSRE.2008.2008278

[6] Y. Sugahara *et al*., "Walking Pattern Generation of a Biped Walking Vehicle Using a Dynamic Human Model," *2006 IEEE/RSJ International Conference on Intelligent Robots and Systems*, Beijing, 2006, pp. 2497-2502. doi: 10.1109/IROS.2006.281695

[7] H. Wang and Y. Li, "Gait planning and control of a biped robot walking up and down stairs," *Shandong Daxue Xuebao (GongxueBan) / Journal of Shandong University (Engineering Science)*, vol. 44, *(2)*, pp. 57-62, 2014. doi: 10.6040/j.issn.1672-3961.0.2013.147

[8] Shih-Kai Chung and J. K. Hahn, "Animation of human walking in virtual environments," *Proceedings Computer Animation 1999*, Geneva, Switzerland, 1999, pp. 4-15. doi: 10.1109/CA.1999.781194

[9] I. Rida, N. Almaadeed and S. Almaadeed, "Robust gait recognition: a comprehensive survey," in *IET Biometrics*, vol. 8, no. 1, pp. 14-28, 1 2019. doi: 10.1049/iet-bmt.2018.5063

[10] D. Chew, D. Gouwanda and A. A. Gopalai, "Investigating running gait using a shoe-integrated wireless inertial sensor," *TENCON 2015 - 2015 IEEE Region 10 Conference*, Macao, 2015, pp. 1-6. doi: 10.1109/TENCON.2015.7373054

[11] H. Qiuyang and Y. Zaiyue, "Frequency-Estimation-Based Thigh Angle Prediction in Level-Ground Walking Using IMUs," *2013 International Conference on Cyber-Enabled Distributed Computing and Knowledge Discovery*, Beijing, 2013, pp. 277-282. doi: 10.1109/CyberC.2013.54

[12] T. Wark, M. Karunanithi and W. Chan, "A Framework for Linking Gait Characteristics of Patients with Accelerations of the Waist," *2005 IEEE Engineering in Medicine and Biology 27th Annual Conference*, Shanghai, 2005, pp. 7695-7698. doi: 10.1109/IEMBS.2005.1616295

[13] T. P. Luu, H. B. Lim, X. Qu, K. H. Hoon and K. H. Low, "Subject-specific lower limb waveforms planning via artificial neural network," *2011 IEEE International Conference on Rehabilitation Robotics*, Zurich, 2011, pp. 1-6. doi: 10.1109/ICORR.2011.5975491

[14] M. Sekine, T. Tamura, M. Akay, T. Fujimoto, T. Togawa and Y. Fukui, "Discrimination of walking patterns using wavelet-based fractal analysis," in *IEEE Transactions on Neural Systems and Rehabilitation Engineering*, vol. 10, no. 3, pp. 188-196, Sept. 2002. doi: 10.1109/TNSRE.2002.802879

[15] J. A. Hughes, J. A. Brown and A. M. Khan, "Smartphone gait fingerprinting models via genetic programming," *2016 IEEE Congress on Evolutionary Computation (CEC)*, Vancouver, BC, 2016, pp. 408-415. doi: 10.1109/CEC.2016.7743823

[16] A. Salarian *et al*., "Gait assessment in Parkinson's disease: toward an ambulatory system for long-term monitoring," in *IEEE Transactions on Biomedical Engineering*, vol. 51, no. 8, pp. 1434-1443, Aug. 2004. doi: 10.1109/TBME.2004.827933

[17] A. Behboodi, H. Wright, N. Zahradka and S. C. K. Lee, "Seven phases of gait detected in real-time using shank attached gyroscopes," *2015 37th Annual International Conference of the IEEE Engineering in Medicine and Biology Society (EMBC)*, Milan, 2015, pp. 5529-5532. doi: 10.1109/EMBC.2015.7319644

[18] H. F. Maqbool, M. A. B. Husman, M. I. Awad, A. Abouhossein, N. Iqbal and A. A. Dehghani-Sanij, "A Real-Time Gait Event Detection for Lower Limb Prosthesis Control and Evaluation," in *IEEE Transactions on Neural Systems and Rehabilitation Engineering*, vol. 25, no. 9, pp. 1500-1509, Sept. 2017. doi: 10.1109/TNSRE.2016.2636367

[19] Y. C. Han, K. I. Wong and I. Murray, "2-Point Error Estimation Algorithm for 3-D Thigh and Shank Angles Estimation Using IMU," in *IEEE Sensors Journal*, vol. 18, no. 20, pp. 8525-8531, 15 Oct.15, 2018. doi: 10.1109/JSEN.2018.2865764

[20] J. A. Zeni, J. G. Richards and J. S. Higginson, "Two simple methods for determining gait events during treadmill and overground walking using kinematic data," *Gait Posture*, vol. 27, (4), pp. 710-714, 2008. doi: 10.1016/j.gaitpost.2007.07.007.

[21] J. De Witt K., "Determination of toe-off event time during treadmill locomotion using kinematic data," *J. Biomech.*, vol. 43, (15), pp. 3067-3069, 2010. doi: 10.1016/j.jbiomech.2010.07.009.

[22] M. A. French, C. Koller and E. S. Arch, "Comparison of three kinematic gait event detection methods during overground and treadmill walking for individuals post stroke," *J. Biomech.*, vol. 99, 2020. doi: 10.1016/j.jbiomech.2019.109481.

[23] C. Senanayake and S. M. N. A. Senanayake, "A computational method for reliable gait event detection and abnormality detection for feedback in rehabilitation," *Comput. Methods Biomech. Biomed.*

Eng., vol. 14, no. 10, pp. 863–874, 2011, doi: 10.1080/10255842.2010.499866.

[24] Y. C. Han, K. I. Wong and I. Murray, "Gait Phase Detection for Normal and Abnormal Gaits Using IMU," in *IEEE Sensors Journal*, vol. 19, no. 9, pp. 3439-3448, 1 May1, 2019. doi: 10.1109/JSEN.2019.2894143

[25] U. Martinez-Hernandez, I. Mahmood, and A. A. Dehghani-Sanij, "Simultaneous Bayesian recognition of locomotion and gait phases with wearable sensors," *IEEE Sensors Journal*, vol. 18, no. 3, pp. 1282–1290, Feb. 2018, doi: 10.1109/JSEN.2017.2782181.